Vietnam Journal of Marine Science and Technology; Vol. 19, No. 3; 2019: 435–447
DOI: https://doi.org/10.15625/1859-3097/19/3/13246
https://www.vjs.ac.vn/index.php/jmst

CFD results on hydrodynamic performances of a marine propeller

Luong Ngoc Loi[1], Nguyen Chi Cong[1,2], Ngo Van He[1,*]

[1]*Hanoi University of Science and Technology, Hanoi, Vietnam*
[2]*Vietnam Maritime University, Hai Phong, Vietnam*
[*]E-mail: he.ngovan@hust.edu.vn

Received: 31 October 2018; Accepted: 5 January 2019

Abstract
In this work, the commercial Computational Fluid Dynamics (CFD), ANSYS-Fluent V.14.5 has been used to illustrate the effects of rudder and blade pitch on hydrodynamic performances of a propeller. At first, the characteristic curves of a container ship propeller are computed. Then, effects of rudder on hydrodynamic performances of the propeller in the both cases of the propeller with and without rudder have been investigated. The relationships between the blade pitch angle and the hydrodynamic performances of the selected referent propeller in this work having designed conditions as diameter of 3.65 m; speed of 200 rpm; average pitch of 2.459 m and the boss ratio of 0.1730. Using CFD, the characteristic curves of the marine propeller, pressure distribution, velocity distribution around propeller and the efficiency of the propeller have been shown. From the obtained results, the effects of rudder and blade pitch angle on hydrodynamic performances of the propeller have been evaluated.

Keywords: CFD, rudder, blade pitch, propeller, hydrodynamic.

Citation: Luong Ngoc Loi, Nguyen Chi Cong, Ngo Van He. CFD results on hydrodynamic performances of a marine propeller. *Vietnam Journal of Marine Science and Technology*, *19*(3), 435–447.

INTRODUCTION

At present, the Computational Fluid Dynamics (CFD) plays important role in simulating flow fields around different geometries using established algorithms. In recent years, considerable advance in the area of computer science has donated to the decrease of computational costs of CFD simulations making it more accessible for practical applications, especially in the process of designing and optimizing ship and propeller.

Simulating the aforementioned experiments provides the opportunity to obtain desired results by analyzing the calculated flow characteristics. It can be a practical way of obtaining valid results at relatively low costs and in reasonable time compared with the real experiments. Since the self-propulsion test simulation is still quite expensive and time demanding, the common practice is to simulate only the open water test and to use its results to determine self-propulsion characteristics. It can be done without taking into account factors including the interaction between the ship hull and the propeller.

Takayuki W. et al., (2003) used the Ansys fluent software to study unsteady cavitation on a marine propeller. In his research, the Reynolds Averaged Navier Stockes (*RANS*) was solved to calculate and analyse the flow around a propeller with cavitation and non-cavitation. The obtained results of his research are that the CFD simulation results were in good agreement with the experiment [1]. Bosschers J. et al., (2008) also used *RANS* method and a boundary element method in which the acoustic wave equation is solved to examine sheet cavitation of propeller and propeller-ship interaction. The achievements of the research were that the computational procedure can give reasonable and good results for the nominal wake field, the cavitation area and the pressure fluctuation on the ship hull. The prediction of fluctuation on the ship hull for model scale was more accurate than for the full scale model [2]. Various numerical methods have been proposed based on potential flow theory for the analysis of propellers. For instance, combination of a panel method which is also known as Boundary Element Method (*BEM*) with a vortex lattice method was utilized to model the propeller [3]. Chen Z. et al., (2015) used the *RANS* method to study the effect of scale on hydrodynamic performances of a propeller and the obtained results are relatively appropriate with experimental outcomes [4]. *RANS* method combined with k-ω turbulent viscous model was used to study the unsteady cavitation turbulent flow around full scale marine propeller [5]. Arnob B. et al., (2017) had got some results relating to computation of hydrodynamic characteristic of marine propeller using induction factor method based on normal induced velocity. The significant results were that the normal induced velocity of a propeller can be obtained simply and accurately by means of the induction factor. The vertical theory based on Biot-Savart law was used to find the induction factor, then the hydrodynamic characteristics of the propeller were estimated [6]. In addition to this area, the important results of simulating, analyzing and optimizing the characteristics of a marine propeller were presented by Hu J. et al., (2017), Lin Y. et al., (2017) and Wang Z. et al., (2012), [7–9]. The obtained results in the studies on effects of geometry configuration on hydrodynamic performances of a propeller proposed the innovative way to design propeller including effects of wake flow and skew angle on propeller's features [10–13]. The other authors got effects of the rudder shape on propeller's hydrodynamic characteristics in the propeller-rudder system [14, 15] from which they suggested the useful way to improve hydrodynamic performances of the propeller. Other authors used the same method with *RANS* and commercial CFD code to investigate the ship hydrodynamics, [16, 17]. In this research, the authors employed the CFD to investigate effect of two factors on the propeller: The first one is effect of a rudder on the propeller's hydrodynamic performance, the second one is effect of the blade pitch on the hydrodynamic features of the propeller.

THEORETICAL FOUNDATION

In this section, the basically theoretical foundation which is applied for CFD computation is shown. These hydrodynamic

coefficients of a free propeller without rudder can be defined as follows [18–20]:

$$K_T = \frac{T}{\rho n^2 D^4};\ K_Q = \frac{Q}{\rho n^2 D^5}$$
$$J = \frac{V_a}{nD};\ \eta_o = \frac{K_T.J}{K_Q.2\pi} \quad (1)$$

Where: J is the advanced ratio; V_a is the axial velocity; n is the rotating speed; D is the diameter of the propeller; T is the thrusts of propeller; Q is the torque of a propeller; ρ is the density of fluid; K_T is the thrust coefficients of propeller; K_Q is the torque coefficient of propeller; and η_o is the efficiency of the ducted propeller.

As we know, a large number of problems involving the fluid are addressed by solving the Navies - Stockes equations to find the field of pressure and velocity distribution and some important parameters. In the paper, the problem was dealt with by utilizing the finite volume method of the commercial CFD code ANSYS- Fluent in which the fundamental equations are the continuity equation and the RANS equation in rotating coordinate system written as follows [2]:

Conservation of mass:

$$\frac{\partial \rho}{\partial t} + \nabla \rho \vec{v}_r = 0 \quad (2)$$

Conservation of momentum:

$$\frac{\partial}{\partial t}\left(\rho \vec{v}_r\right) + \nabla\left(\rho \vec{v}_r.\vec{v}_r\right) + \rho\left(2\vec{\omega}\times\vec{v}_r + \vec{\omega}\times\vec{\omega}\times\vec{r} + \vec{a}\times\vec{r} + \vec{a}\right) = -\nabla p + \nabla\bar{\bar{\tau}} + \vec{F} \quad (3)$$

Where: $\vec{a} = \frac{d\vec{\omega}}{dt}$ and $\vec{a} = \frac{d\vec{v}_t}{dt}$.

The stress tensor $\bar{\bar{\tau}}$ is given by:

$$\bar{\bar{\tau}} = \mu\left[\left(\nabla\vec{v} + \nabla\vec{v}^T\right) - \frac{2}{3}\nabla\vec{v}^I\right] \quad (4)$$

The momentum equation contains four additional acceleration terms. The first two terms are the Coriolis acceleration ($2\vec{\omega}\times\vec{v}_r$) and the centripetal one ($\vec{\omega}\times\vec{\omega}\times\vec{r}$), respectively. These terms appear for both steadily moving reference frames (that are constant) and accelerating reference frames (that are functions of time). The third and fourth terms are due to the unsteady change of the rotational speed and linear velocity, respectively. These terms vanish for constant translation and/or rotational speeds.

MODELS AND CONDITIONS

In this section, to investigate the effects of the rudder and blade pitch angle on hydrodynamic performance of the propeller, the authors carried out the specific cases as follows:

The first case: To cope with effects of blade pitch on the propeller' hydrodynamic features, the team employed the calculation and simulation of the free propeller with advance ratio J changing from 0.1 to 0.75 and attack angle of the blade in the range of -7 degree to 7 degrees.

The second case: To study effects of rudder on hydrodynamic characteristics of the propeller, the authors executed the computation of the free propeller and propeller in the rudder propeller system with advance ratio J changing from 0.1 to 0.75.

The studied propeller and rudder are equipped in the Tan Cang Foundation container ship. The dimension parameters of the propeller and rudder are given in tables 1–2. The rudder is installed after propeller and the position between rudder and propeller is shown in fig. 1.

Table 1. Principal parameters of propeller

Parameter	Value	Unit
Diameter	3.65	m
Pitch	2.459	m
Revolution	200	rpm
Number of blades	4	
Cross section	Naca 66, a = 0.8	
Rake	10	Deg
Screw	25	Deg

Table 2. Principal dimension of duct

Parameter	Value	Unit
Rudder height	4.8	m
Chord length of top section	3.45	m
Chord length of bottom section	2.45	m
Rudder area	12	m^2
Rudder profile	NaCa 0018	

Characteristic curves of a propeller consist of the three curves, that are thrust, torque and efficient curves corresponding to the different advance velocities. To construct those curves of the investigated propeller by the CFD, the first step in process is to build the suitable computed fluid domain. In this research, the domain is a cylinder, with the length of thirteen times of the propeller's diameter (13D) and the diameter of seven times (7D) of the propeller's diameter, divided by the two components: The static domain and rotating domain. In the third step, the domain is imported, meshed, and refined in the Ansys meshing ICEM-CFD tool. All domains are meshed by using tetra unstructured mesh in which the rotating domain is modeled with smooth mesh, and the static domain takes the coarse one, then they are converted into polyhedral mesh to save calculation time and improve accuracy for simulation results.

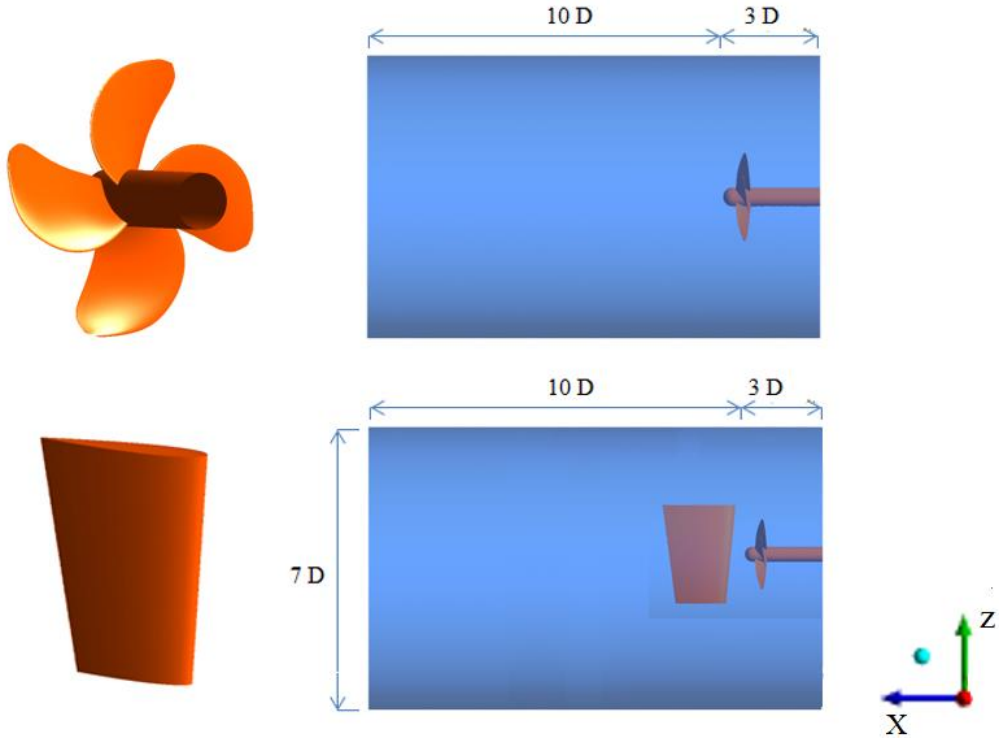

Fig. 1. Computational fluid domain

The quality of computational grid plays important role and directly affects the convergence and results of numerical analysis. To determine mesh independence on calculation results, the team employed calculations for nine different numbers of mesh to specify the suitable number of mesh. These calculations are carried out at the advance ratio J of 0.2 and the dependence of mesh number with the calculation results in the two cases, the free propeller without rudder and the propeller with rudder in one system as shown in the fig. 1. We can see that the mesh number for all the computations has to be larger than 325000 polyhedral elements to ensure the accuracy, so the authors finally selected the five cases in which the mesh element number in the two cases is 631646 and 682736 elements respectively for all calculations. The geometry, investigated domain and mesh are shown in fig. 2.

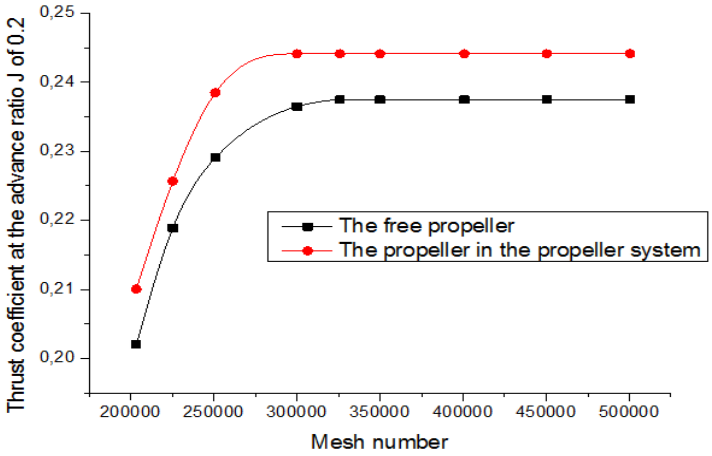

Fig. 2. Mesh independence for computation

Table 3. Detailed mesh for computation

Domain	Nodes	Elements	Polyhedral mesh
Free propeller - without rudder			
Dynamic fluid	326437	326437	326437
Static fluid	305209	305209	305209
All domain	631646	631646	631646
Propeller - rudder system			
Dynamic fluid	326437	326437	326437
Static fluid	356299	356299	356299
All domain	682736	682736	682736

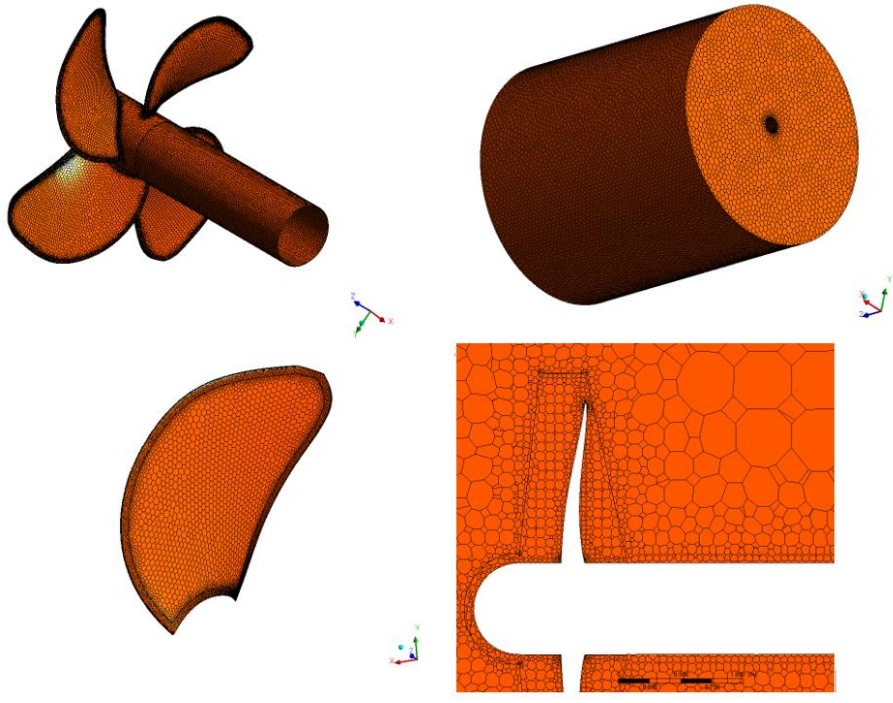

Fig. 3. Mesh of the free propeller case

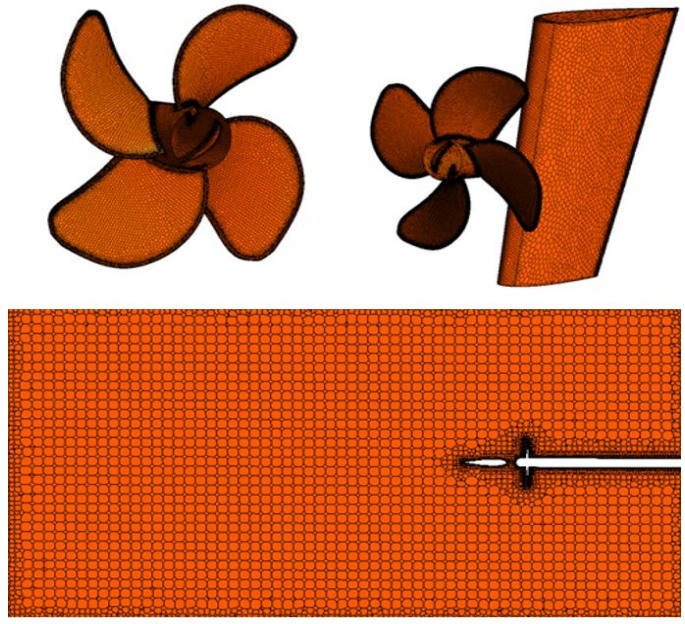

Fig. 4. Mesh of the propeller - rudder system

In computation, the turbulent viscous model *RNG k-ε* is used. Velocity inlet, which is axially uniform and has magnitude equal to the ship's advance velocity, is selected as the inlet. Pressure outlet is specified as the outlet and gauge pressure on the outlet is set to be 0 Pa. With wall boundary condition, no slip condition is enforced on wall surface and standard wall function is also applied to adjacent region of the walls. Moving reference frame (*MRF*) is used to establish the moving coordinate system rotating with the propeller synchronously and the stationary coordinate system fixed on static shaft of the propeller, respectively. The first order upwind scheme with numerical under-relaxation is applied for the discretization of the convection term and the central difference scheme is employed for the diffusion term. The pressure - velocity coupling is solved through the PISO algorithm [21, 22]. The detailed conditions are shown in table 4.

Table 4. Computed condition setup for simulation

Name	Conditions	Value	Unit
Inlet	Velocity inlet	1.22-9.15	m/s
Outlet	Pressure inlet	0	pa
Wall	Static wall	-	-
Static domain	Static fluid	-	-
Dynamic domain	Rotating	200	rpm

CFD RESULTS AND ANALYSIS

In this section, the CFD results of hydrodynamic performances of the propeller are shown. Fig. 5 shows the pressure distribution on the back and pressure face of the propeller at the different advance ratios *J* from 0.1 to 0.6. The principle of pressure distribution on the two faces of the blade satisfies the theoretical law of the axial turbo machinery. There is the pressure difference between the pressure face and the back face of the propeller in operation, and that difference makes the propeller thrust overcome the ship hull resistance. The pressure distribution on the two faces of the blade mainly depends on the advance ratio J or velocity inlet, the smaller the advance ratio, the higher the thrust. At the operating condition of the ship $J = 0.6$, on the pressure face, almost all the area of the blade has the pressure value of about 2.4×10^4 Pa, while almost all area of the suction face has the pressure in the range of -4×10^4 Pa. This means that the fluid accelerates as it approaches the propeller due to low pressure in the front of the propeller and the water continues to accelerate when it leaves the propeller.

Fig. 6 shows CFD results of hydrodynamic performance curves of the propeller corresponding to the different advance ratios *J*.

As we can be seen from the figure, the changing principle of thrust and torque coefficient decreases gradually when the advance ratio *J* raises, and the maximum thrust and torque coefficients are 0.283, 0.032 respectively at the advance ratio *J* of 0.1. The efficiency curve is slightly different in which it conforms to the linear principle with small advance ratio in range of 0.1–0.4, and the maximum efficiency is 0.66 with advance ratio *J* of 0.6 at the initially designed optimal point.

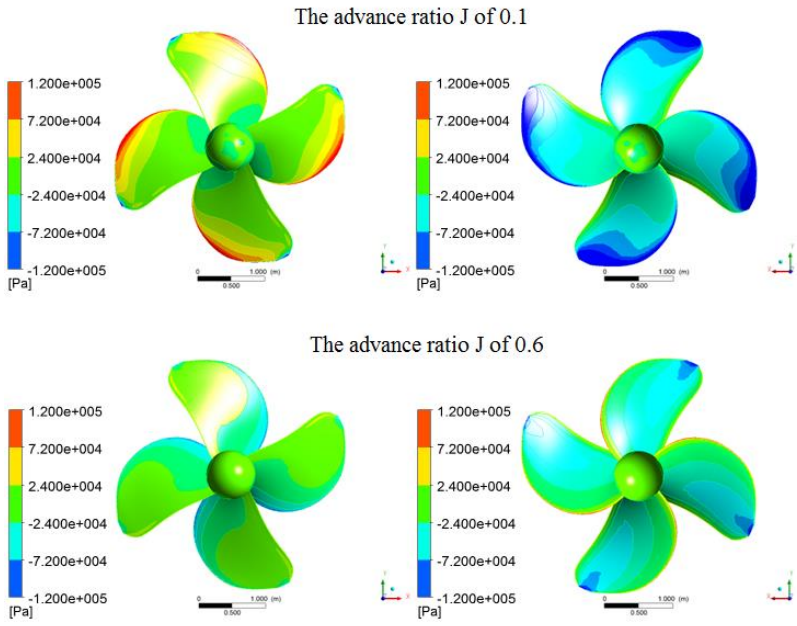

Fig. 5. Pressure distribution over blades surface of propeller at J of 0.1 and 0.6

In this section, the effects of rudder in the rudder-propeller system on hydrodynamic performances of the propeller are investigated by using the numerical method. The two models of the propeller with and without rudder are computed in the same condition to compare the hydrodynamic performances. Fig. 6 shows the CFD results of pressure distribution on the propeller's faces at advance ratio *J* of 0.6.

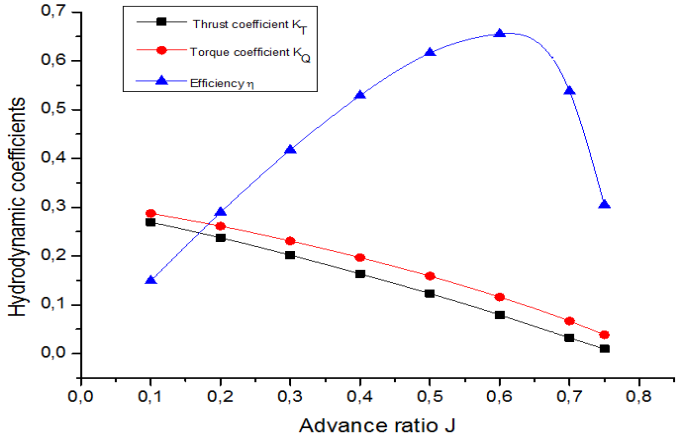

Fig. 6. The characteristic curves of the propeller

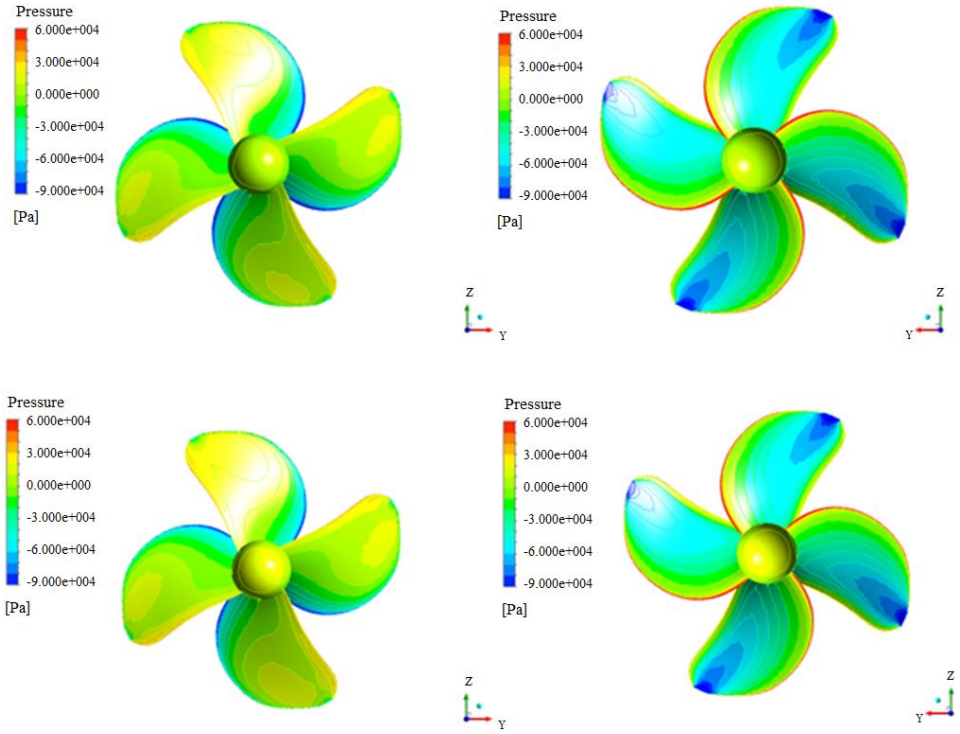

Fig. 7. Pressure distribution over blade surface of the propeller in both cases at $J = 0.6$

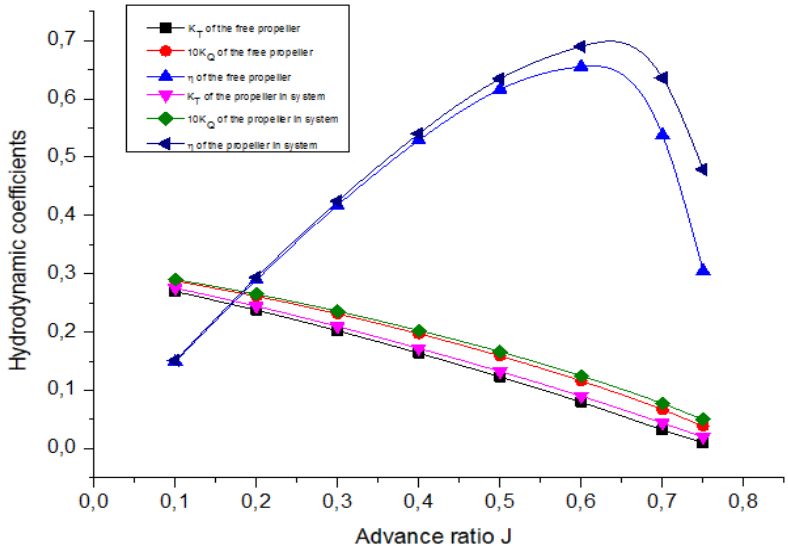

Fig. 8. The characteristic curves of the propeller with and without rudder

Fig. 7 reveals the pressure distribution on the back face and pressure face of the propeller in the both cases at the advance ratio J of 0.6. As can be seen, the pressure distribution on the back face of the propeller in both cases is relatively similar while the pressure distribution on the pressure face of the propeller in the propeller-rudder system and the open-water propeller is slightly different especially at the region of the propeller hub. In the propeller-rudder system, the propeller thrust goes up compared with the open-water propeller

because the low-pressure area on the hub decreases and the pressure face's high-pressure area near the blade's tip increases. The pressure value at this region is about -1.2×10^{-4} Pa. The propeller's thrust in this case also increases, however the raise of the propeller thrust is higher than the increase of the torque acting on the propeller. As the result, the propeller efficiency in the propeller - rudder goes up slightly. Fig. 8 reveals the characteristic curves of the propeller in the cases. From the figure, we can recognize that the efficiency of the propeller in the propeller - rudder system is slightly higher than the efficiency of the free propeller. The higher advance ratio the vessel gets, the higher efficiency the propeller obtains. At the designed optimal point of the propeller corresponding to the exploited velocity of the vessel, the propeller's efficiency in the propeller-rudder system increases by about 4.8 percentages.

Effects of propeller on the rudder's hydrodynamic features are investigated by the CFD. Fig. 9 presents the vector velocity going out the propeller and pressure distribution of the rudder's faces. It can be seen from the figure that velocity field after the propeller is not uniform, and flow's vector inclines with the rudder's symmetry plane with any angle. This makes pressure distribution of rudder faces asymmetric and the maximum pressure gets about 6×10^4 Pa at the region corresponding to the propeller's blade tips. As the results, not only the drag acts on the rudder but also the vertical force appears on the rudder. The rudder's drag changes in a nearly linear function of advance ratio *J*, and the maximum drag of the rudder is 16 kN at the advance ratio *J* of 0.75. On the other hand, the vertical force is a curve of advance ratio *J*, it gets the maximum value about 4 kN corresponding to *J* of 0.5. At the small velocity, it increases dramatically, while at the advance ratio *J* in the range of 0.5–0.75, it decreases slightly. The changing principle of forces is given in fig. 10.

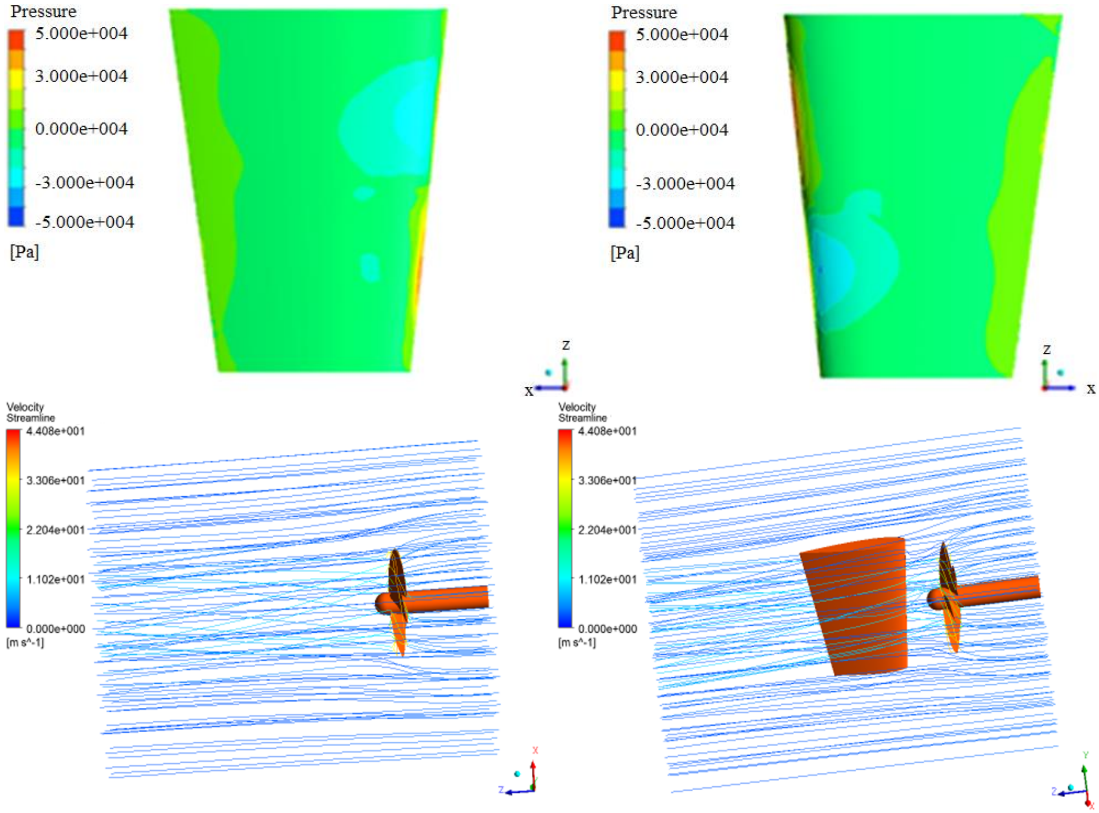

Fig. 9. Pressure distribution over rudder surface and flow around rudder

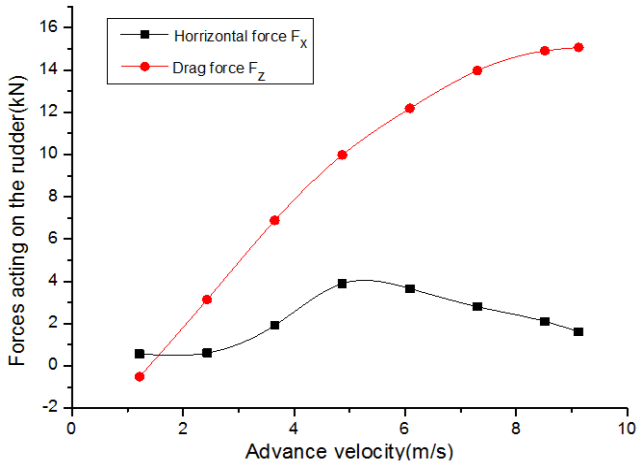

Fig. 10. Hydrodynamic force acting on the rudder

In this paper, the numerical method is used to investigate effects of blade pitch on hydrodynamic performances of the propeller. The blade pitch angle is changing from -7 degree to 7 degrees. The computational condition is the same for all the models. Fig. 11 shows the results of pressure distribution on faces with different blade pitches at the advance ratio *J* of 0.4.

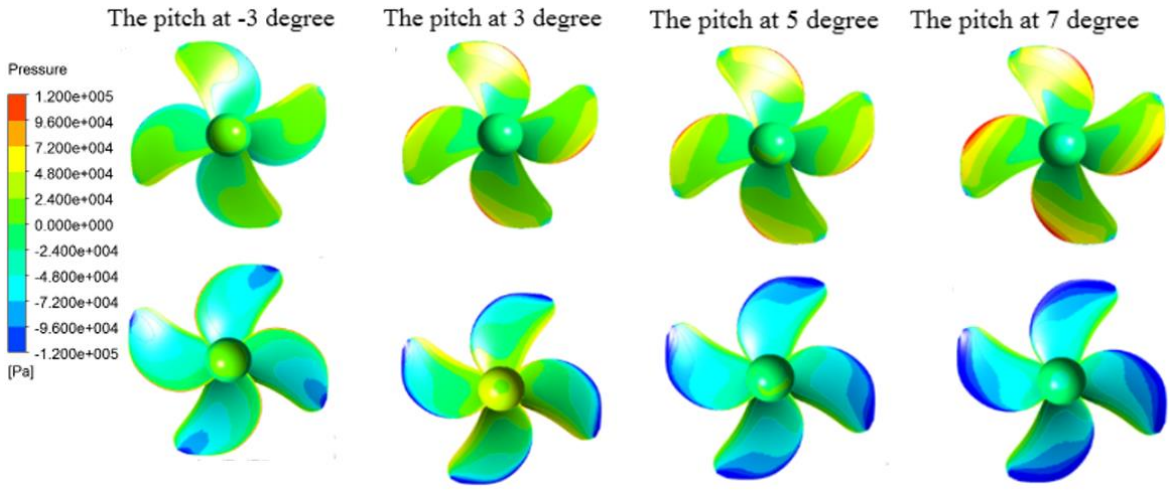

Fig. 11. Pressure distribution over blade surface of propeller with different blade pitch angles

As we can see in the fig. 11, the blade pitch has a significant impact on pressure distribution of the propeller blade's surfaces. Consequently, the propeller thrust increases steadily when the blade pitch rises. Fig. 12 shows propeller efficiency at the different blade pitch angles. We can see from the figure that the propeller efficiency changes to the principle of the axial turbomachinery and it is a function of the advance ratio J at each pitch. In the investigated pitches, the propeller efficiency goes up dramatically when the blade pitch increases. The maximum efficiency of the propeller is 0.724 corresponding to the advance ratio *J* of 0.8 at the blade pitch of 7 degrees. However, at the specific pitch, the propeller efficiency always has the extremum corresponding to the specific advance ratio *J*. This is meaningful with the controllable pitch propellers in which

its blade pitch can change to adjust to load acting on a vessel in the operation. With a propeller of this type, the general characteristic curve is a set of the characteristic curves at different pitch ratios, so in each specific operating condition of a ship, the propeller can change the blade pitch to get high efficiency without altering the revolution of the engine shaft.

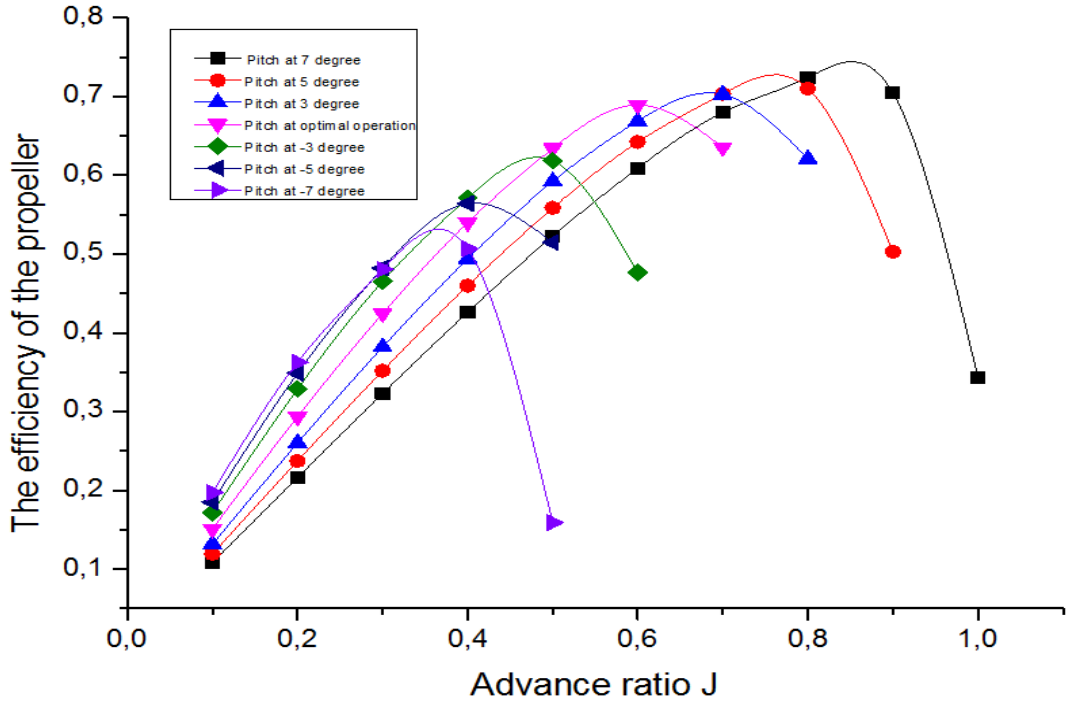

Fig. 12. Efficiency of the propeller with the different blade pitch angles

CONCLUSIONS

In this paper, the propeller and rudder of the Tan Cang Foundation ship are analyzed at different advance ratios to construct the hydrodynamic performance curves. The effects of rudder and blade pitch angle of the propeller are investigated and these are some obtained results in the paper.

The characteristic propeller curves are constructed by using *MRF* and *RNG k-ε* model in the Ansys Fluent 14.5. The maximum efficiency of the propeller is 0.66 with open water propeller and is 0.689 with the rudder - propeller system at the advance ratio 0.6.

The obtained results reveals that the rudder has slight effect on the propeller's hydrodynamic characteristics. At the designed optimal point of the studied propeller, the efficiency in the rudder-propeller system goes up about 4 percentages compared with the open-water propeller. On the contrary, the propeller also has significant impact on the hydrodynamic features of the rudder. The interaction between the propeller and the rudder makes the horizontal force on the rudder in the ship operation, this force reaches the maximum value of 4.5 kN at corresponding to the advance ratio J = 0.4. The force generating on this interaction reduces the stability of the ship's maneuvering.

The blade pitch also has important effects on the hydrodynamic characteristics of the propeller. When the blade pitch goes up, in the investigated pitch, the thrust and torque coefficients of the propeller increase dramatically. This is important foundation to calculate and design the controllable pitch propeller in which its blade pitch can change in operation. The general characteristic curve of this type of propeller is a set of the curves at the

different pitches, so the ship equipped with a controllable pitch operating in the specific condition usually gets the high efficiency when compared with the fixed propeller having the same geometry characteristics.

Acknowledgements: This research is funded by Hanoi University of Science and Technology (HUST) under grant number T2018-PC-045.

REFERENCES

[1] Wang, Z., Xiong, Y., and Qi, W., 2012. Numerical prediction of contra-rotating propellers' open water performance. *Huazhong Keji Daxue Xuebao(Ziran Kexue Ban)/Journal of Huazhong University of Science and Technology(Nature Science Edition)*, *40*(11). 77–88.

[2] Bosschers, J., Vaz, G. N. V. B., Starke, A. R., and van Wijngaarden, E., 2008. Computational analysis of propeller sheet cavitation and propeller-ship interaction. In *Proceedings of the RINA Conference "MARINE CFD2008", Southampton, UK* (pp. 26–27).

[3] Watanabe, T., Kawamura, T., Takekoshi, Y., Maeda, M., and Rhee, S. H., 2003. Simulation of steady and unsteady cavitation on a marine propeller using a RANS CFD code. In *Proceedings of The Fifth International Symposium on Cavitation*.

[4] Chen, Z., 2015. CFD Investigation in Scale Effects on Propellers with Different Blade Area Ratio. *The master thesis at Aalesund University College*, 2015. Pp. 1–71.

[5] Ji, B., Luo, X. W., Wu, Y. L., Liu, S. H., Xu, H. Y., and Oshima, A., 2010. Numerical investigation of unsteady cavitating turbulent flow around a full scale marine propeller. *Journal of Hydrodynamics, Ser. B*, *22*(5), 747–752. Doi: 10.1016/s1001-6058(10)60025-x.

[6] Banik, A., and Ullah, M. R., 2017. Computation of Hydrodynamic Characteristics of A Marine Propeller Using Induction Factor Method Based on Normal Induced Velocity. *Procedia engineering*, *194*, 120–127.

[7] Hu, J., Li, T., Lin, Y., Ji, Z., and Du X., 2017. Numerical simulation of open water performance of B series of contra-rotating propellers based on RANS methods. *Journal of Dalian University of Technology*, *57*(2), 148–156.

[8] Lin Y., Rao Z., Yang C., 2017. Hydrodynamic optimization of a seven-bladed propeller with skew. *Journal of Shipbuilding of China*, *57*(4), 1–13.

[9] Ommundsen, A., 2015. Unconventional Propeller Tip Design. In *Norwegian University of Science and Technology*.

[10] Belhenniche, S., Aounallah, M., Omar, I., and Çelik, F., 2016. Effect of geometric configurations on hydrodynamic performance assessment of a marine propeller. *Brodogradnja: Teorija i praksa brodogradnje i pomorske tehnike*, *67*(4), 31–48. Doi: 10.21278/brod67403.

[11] Brizzolara, S., Gaggero, S., and Grassi, D., 2013. Hub effect in propeller design and analysis. In *Third International Symposium on Marine Propulsors* (pp. 110–119).

[12] Ghasemi, H., 2009. The effect of wake flow and skew angle on the ship propeller performance.

[13] Kuiper, G., 2010. New developments and propeller design. *Journal of Hydrodynamics, Ser. B*, *22*(5), 7–16. Doi: 10.1016/s1001-6058(09)60161-x.

[14] Ngo, V. H., Le, T. T., Le, Q., and Ikeda, Y., 2015. A study on interaction effects on hydrodynamic performance of a system rudder-propeller by distant gap. *Proceedings of the 12th International Marine Design Conference, Tokyo, Japan*. Pp. 179–193.

[15] Ngo, V. H., Le, T. T., and Ikeda, Y., 2016. A study on improving hydrodynamic performances of a system rudder and propeller by attaching a fix plate on the rudder. *The 8th Asia-Pacific Workshop on Marine Hydrodynamics - APHydro 2016, Hanoi, Vietnam*. Pp. 277–284.

[16] Anh Tuan, P., 2012. Hydrodynamics of Autonomous Underwater Vehicles. *Journal of Mechatronics*, *1*(1), 25–28. Doi: 10.1166/jom.2012.1002.

[17] Phan, A. T., 2016. A Study on Hovercraft Resistance Using Numerical Modeling. *Applied Mechanics and Materials*, *842*, 186–190. DOI: https://doi.org/10.4028/www.scientific.net/AMM.842.186.

[18] Carlton, J., 2012. Marine Propellers and Propulsion. *Butterworth-Heinemann*. ISBN: 9780080971247. Pp. 1–544.

[19] Abbott, I. H., and Von Doenhoff, A. E., 1959. Theory of wing sections, 1959. *Google Scholar*, 112–115.

[20] Breslin, J. P., and Andersen, P., 1996. Hydrodynamics of ship propellers (Vol. 3). *Cambridge University Press*.

[21] ANSYS Fluent Theory Guide. 2013. https://www.ansys.com/products/fluids/ansys-fluent.

[22] ITTC, 2011. The proc. of the 26th International Towing Tank Conference, Rio de Janeiro, Brazil, Website: http://ittc.sname.org/proc26/assets/documents/VolumeI/Proceedings-Vol-01.pdf.

[23] Mizzi, K., Demirel, Y. K., Banks, C., Turan, O., Kaklis, P., and Atlar, M., 2017. Design optimisation of Propeller Boss Cap Fins for enhanced propeller performance. *Applied Ocean Research*, *62*, 210–222.

[24] Phan, A. T., 2016. A Study on Hovercraft Resistance Using Numerical Modeling. *Applied Mechanics and Materials*, *842*, 186–190. DOI: https://doi.org/10.4028/www.scientific.net/AMM.842.186.

[24] Lee, S. K., 2008. Ice Controllable Pitch Propeller Strength Check Based on IACS Polar Class Rule. In *Originally Presented at the Ice Tech Conference Held July*, (pp. 20–23).

[25] Van He, N., and Ikeda, Y., 2013. Optimization of bow shape for a non ballast water ship. *Journal of Marine Science and Application*, *12*(3), 251–260. DOI: 10.1007/s11804-013-1196-8.

[26] Van He, N., and Ikeda, Y., 2014. Added resistance acting on hull of a non ballast water ship. *Journal of Marine Science and Application*, *13*(1), 11–22. DOI: 10.1007/s11804-014-1225-2.

[27] Van He, N., Mizutani, K., and Ikeda, Y., 2016. Reducing air resistance acting on a ship by using interaction effects between the hull and accommodation. *Ocean Engineering*, *111*, 414–423. DOI: 10.1016/j.oceaneng.2015.11.023.

[28] Cong, N. C., Loi, L. N., and Van He, N., 2018. A Study on Effects of Blade Pitch on the Hydrodynamic Performances of a Propeller by Using CFD. *Journal of Shipping and Ocean Engineering*, *8*, 36–42. DOI: 10.17265/2159-5879/2018.01.005.

[29] Kinnas, S. A., Tian, Y., and Sharma, A., 2012. Numerical modeling of a marine propeller undergoing surge and heave motion. *International Journal of Rotating Machinery*, *2012*, 257461. https://doi.org/10.1155/2012/257461.

[30] ITTC, 2008. The proc. of the 25th International Towing Tank Conference, Fukuoka, Japan, Website: http://ittc.sname.org/proc25/assets/documents/VolumeI/Proceedings-Vol-01.pdf.